Published by AIT
the Italian Society of Remote Sensing

# On the use of COSMO/SkyMed data and Weather Models for interferometric DEM generation

**Davide Oscar Nitti[1,2], Fabio Bovenga[3]*, Raffaele Nutricato[1,2], Francesca Intini[1,2] and Maria Teresa Chiaradia[1]**

[1]Dipartimento Interateneo di Fisica, Politecnico di Bari, Via Amendola 173, 70126 Bari, Italy
[2]GAP srl, c/o Dip. Interateneo di Fisica, Politecnico di Bari, Via Amendola 173, 70126 Bari, Italy
[3]National Research Council of Italy, CNR-ISSIA, Via Amendola 122/D, 70126 Bari, Italy
*Corresponding author, e-mail address: bovenga@ba.issia.cnr.it

## Abstract
This work experiments the potentialities of COSMO/SkyMed (CSK) data in providing interferometric Digital Elevation Model (DEM). We processed a stack of CSK data for measuring with meter accuracy the ground elevation on the available coherent targets, and used these values to check the accuracy of DEMs derived from 5 tandem-like CSK pairs. In order to suppress the atmospheric signal we experimented a classical spatial filtering of the differential phase as well as the use of numerical weather prediction (NWP) model RAMS. Tandem-like pairs with normal baselines higher than 300 m allows to derive DEMs fulfilling the HRTI Level 3 specifications on the relative vertical accuracy, while the use of NWP models still seems unfeasible especially for X-band.

**Keywords:** SAR Interferometry, COSMO/SkyMed, numerical weather model.

## Introduction
Digital Elevation Model (DEM) products for Earth observation space-borne applications are being to play a role of increasing importance due to the new generation of high resolution sensors (both optical and SAR). These new sensors demand elevation data for processing and, on the other hand, they provide new possibilities for DEM generation. Till now, for what concerns interferometric DEM, the Shuttle Radar Topography Mission (SRTM) has been the reference product for scientific applications for regions between -54 and 60 degrees latitude. SRTM mission [Rabus et al., 2003] had the challenging goal to meet the requirements for a homogeneous and reliable DEM fulfilling the DTED-2 specifications [NIMA, 2000]: 12÷15 m of relative vertical accuracy, 18 m of absolute vertical accuracy and 30 m of spatial resolution. However, the new generation of high resolution sensors (including SAR) pose new requirements for elevation data in terms of vertical precision and spatial resolution. DEM are usually used as ancillary input in different processing steps as for instance geocoding and Differential SAR Interferometry (DInSAR). In this context,

the recent SAR missions TerraSAR-X (TSX) and TanDEM-X (TDX) from DLR, as well as COSMO/SkyMed (CSK) constellation from ASI can play a promising role thanks to their high resolution both in space and time. In a formation flight at distances of a few kilometers down to less than 200 meters, TSX (in orbit since June 2007) and TDX (launched in 2010) are synchronously recording data in Stripmap Mode (3 m of spatial resolution), with the aim of providing a DEM for the whole Earth surface fulfilling the HRTI Level 3 specifications [Krieger et al., 2007]: 2÷4 m of relative vertical accuracy, 10 m of absolute vertical accuracy and 12 m of spatial resolution.

CSK mission is instead a constellation of four satellite SAR sensors, designed for ensuring Earth monitoring with a short revisit time (up to 12 hours for the full CSK constellation) [Battazza et al., 2009; Covello et al., 2010]. Recent scientific works [Bovenga et al., 2012; Reale et al., 2011] have shown the advantages of using CSK in the monitoring through SAR interferometry (InSAR) terrain deformations caused for instance by landslides and earthquakes. Moreover, this mission, as the TSX and the Radarsat-2 missions, provides spatial resolutions from 1 m to 3 m (for Spotlight and Stripmap modes respectively), i.e. one order of magnitude better than the previously available satellite SAR data. Thanks to the high spatial resolution, CSK appears to be very promising in monitoring man-made structures, such as buildings, bridges, railways and highways, thus enabling new potential applications (urban applications, precise DEM, etc.). The present work investigates the potentialities of the CSK constellation for ground elevation measurement with particular attention devoted to checking the possibility of meeting the HRTI Level 3 specifications for DEM generation.

Actually, CSK offers a "tandem-like" interferometry configuration. Differently than a tandem configuration, where the satellites are flying in close proximity (as for TSX and TDX), the "tandem-like" one consists in a "one-day" relative phasing between a satellite couple [Covello et al., 2010]. Thanks to the wide range bandwidth (up to more than 300 MHz for Spotlight acquisitions) CSK interferometric pairs are usually affected by a limited relative spectral shift and consequent geometrical decorrelation [Zebker and Villasenor, 1992]. Hence, the main issue in the exploitation of CSK interferometric products for topographic mapping is represented by both temporal decorrelation and atmospheric phase artifacts [Hanssen, 2001].

In the case of high coherence and assuming no movement and successful orbital error removal, the main problem in height computation derives from the atmospheric contribution. Different strategies can be adopted to filter out this signal. By processing a stack of images and through advanced multi-temporal interferometric analysis [Ferretti et al., 2001; Berardino et al., 2001] it is possible to identify targets on the ground which behave coherently in time. For these persistent scatterers (PS), besides the displacement, also the elevation can be measured reaching metric accuracy [Perissin and Rocca, 2006]. These techniques allow to filter out the atmospheric signal thanks to its decorrelation in time and correlation in space. The main drawback is related to the availability of coherent targets on the area of interest. It was demonstrated [Bamler et al., 2009; Prati et al., 2010; Bovenga et al., 2012] that high resolution SAR sensors (such as CSK) allow to increase the density of the measurable targets, making this approach to height measurement valuable.

Another possible strategy consists of processing tandem-like high resolution interferometric pairs through a standard interferometric processor. In order to identify and remove the

atmospheric artefacts, the differential phase field can be generated by subtracting the reference height derived by a low resolution DEM as, for instance, the SRTM product at 3 arcsec (resolution cell of 90x90 $m^2$). Then, provided that a strong height sensitivity is available, the phase contributions related to atmosphere and to the residual topography can be separated by using either *ad hoc* high-pass filtering or the outcomes of a Numerical Weather Prediction (NWP) model. The estimated residual topography may hence improve the accuracy of the reference DEM.
The stacking approach [Sandwell and Sichoix, 2000] can also be used to filter out the atmospheric artifacts through a temporal average of several independent DEM's. However, it is really uncommon to have an adequate number of tandem-like pairs to perform a reliable atmospheric signal suppression.
In recent years the use of NWP modelling in the framework of SAR interferometry has been increasingly experimented showing in general good agreement for the long wavelength features, but not for small turbulent processes [Pielke et al., 1992]. One of the problems arising when using NWP models is that the spatial resolution does not match that of SAR data in particular when dealing with high resolution sensors (as CSK). Further investigations concerning this issue are generally claimed.
This work presents results obtained by processing high resolution CSK acquisitions through standard SAR Interferometry as well as multi-pass interferometry with the aim of measuring ground elevation. Moreover, we investigated the feasibility of using NWP modelling to mitigate the atmospheric artefacts affecting the interferometric phase.
We first processed through the SPINUA algorithm [Bovenga et al., 2004] a stack of CSK data acquired over Parkfield (California, USA), measuring with meter accuracy the ground elevation of available coherent targets. Then we used this set of measurements as reference values to check the accuracy of the height inference obtained by processing 5 tandem-like CSK Spotlight pairs with different values of the normal baseline (and accordingly height sensibilities). The results are analysed with respect to the HRTI Level 3 specifications for DEM generation. We also attempted to support the tandem-like CSK processing by using the interferometric atmospheric phase contribution estimated by using the NWP model named RAMS (Regional Atmospheric Modeling System) [Pielke et al., 1992]. NWP model outputs were also validated by using radiosonde records as well as GPS measurements.

## Multi-temporal interferometric analysis for height measurements

Multi-temporal interferometric analysis, as Persistent Scatterer Interferometry (PSI) [Ferretti et al., 2001], provides the following products: i) the displacement signal occurred within the time interval covered by the images; ii) the atmospheric component affecting each image also known as Atmospheric Phase Screen (APS); iii) the residual topographic error computed with respect to the DEM used in the processing. This latter can be used to refine the DEM on the PS and, consequently, to improve the geocoding of PSI products. The accuracy of target positioning achievable by means of the interferometric multi-temporal analysis has been proved, by using ERS and ENVISAT SAR data, to be in the order of 1 m in the three dimensions [Perissin and Rocca, 2006]. Even though a quantitative evaluation of the positioning is not still available in the case of high resolution X-band PSI, it appears to be even better than for the C-band medium resolution data due to the higher spatial resolution, the shorter wavelength and the improved phase quality [Crosetto et al., 2010].

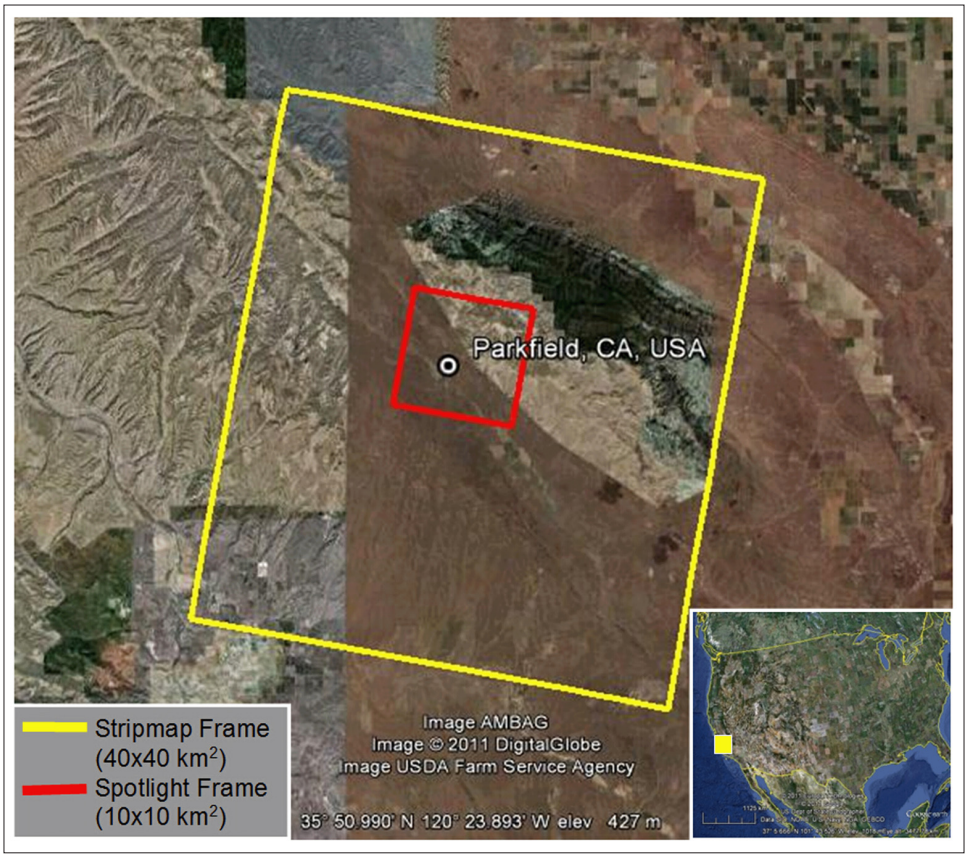


**Figure 1 - Yellow and red frames refer respectively to the Stripmap and Spotlight CSK images ground coverage. Background optical image is from Google Earth (GE).**

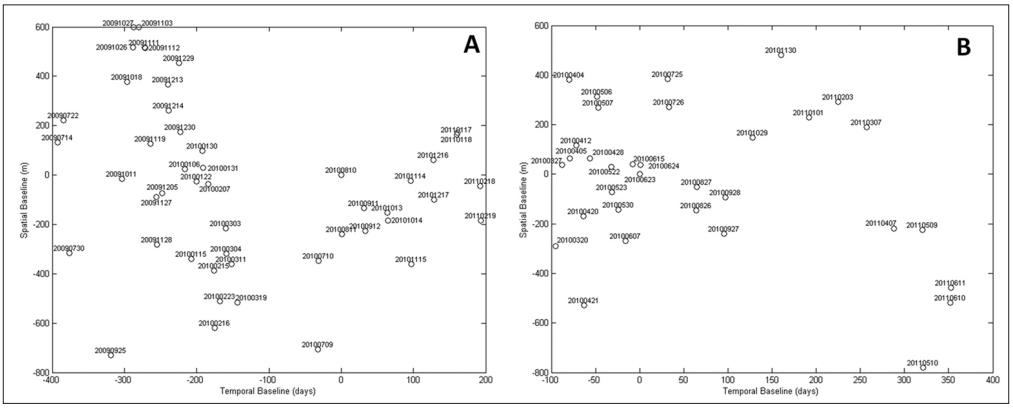


**Figure 2 - Spatial and temporal baseline distribution for (A) stripmap and (B) spotlight dataset. The reference time is set to the acquisition date of master image: 10.08.2010 for the spotlight dataset (A) and 23.06.2010 for the Stripmap dataset (B).**

The CSK constellation acquires data from its four SAR X-band satellites in several imaging modes providing different spatial resolutions, polarizations and ground coverage. For the present study, we processed two stacks of CSK images acquired over Parkfield (California, USA) (see Fig. 1) both in Stripmap and Spotlight modes with resolution cell's sizes of 3x3 $m^2$ and 1x1 $m^2$ respectively. Thanks to the high spatial resolution, high accuracy is expected for the height measurements which can then be used as reference values to check the accuracy of the DEM obtained by the differential interferometric processing of tandem-like pairs.
The Stripmap dataset (yellow frame in Figure 1) consists of 48 right-looking images acquired between July, 2009 and February 2011 along descending pass in VV polarization at a look angle of 30.6 deg (beam H4-05). The Spotlight dataset (red frame in Figure 1) consists of 33 right-looking images acquired between March, 2010 and June 2011 along descending pass in VV polarization at a look angle of 30.9 deg (beam ES-08). Figure 2 shows the scatter plot of the temporal ($B_t$) and spatial ($B_n$) baselines for the Stripmap (A) and the Spotlight datasets (B).
Different studies [Bamler et al., 2009; Prati et al., 2010; Bovenga et al., 2012] already proved that by increasing the spatial resolution of the SAR sensor the density of the coherent targets increases as well. According to this statement, we used the heights computed by processing the Spotlight dataset as reference values for the following analysis, while the result coming from the Stripmap dataset was used to cross-validate the PSI processing.
PSI processing was performed through the SPINUA (Stable Point INterferometry over Un-urbanised Areas) algorithm [Bovenga et al., 2004; Bovenga et al., 2006]. The processing chain is the result of a joint effort of the Remote Sensing Group of the Department of Physics at *Politecnico di Bari* and the ISSIA-CNR institute of Bari. SPINUA has been developed with the aim of detecting and monitoring coherent PS targets in non- or scarcely-urbanized areas. The processing chain has been further updated in order to deal properly with X-band data from both CSK and TSX.
PSI processing was carried out by using a an SRTM DEM at 1 arcsec which has a resolution size of 30 x 30 $m^2$. The ground elevation ranges from 450 m up to 950 m. Although 500 m of topography variation is not the optimum for a study aimed at evaluating the performance of DEM reconstruction, this test site provides the uncommon opportunity to have available two multi-temporal CSK datasets as well as several Spotlight tandem-like pairs.
Figure 3 shows the residual topographic error map computed with respect to SRTM DEM at 1 arcsec by processing the Spotlight (left) and Stripmap (right) datasets. Although the site is non urbanized, the PSI results show good coverage of the area of interest, especially in the case of Spotlight data which provides a density of more than 70000 PS/$km^2$. In the case of Stripmap data the density drops down to 2200 PS/$km^2$. The areas suffering of PS-lack coincide mainly with vegetation cover or slopes affected by layover and shadowing.
Both datasets were acquired along descending passes with the same incident angle, thus ensuring the proximity of the scattering centre measured by the two acquisition modes on the same coherent targets on the ground. Hence, the PSI measurements can be validated by a cross comparison between the results obtained by processing the two independent datasets. Figure 4-A and Figure 4-B show respectively the histogram of the height differences and the scatter plot between the height values derived by processing the two datasets. The correlation coefficient of 0.99 proves the good agreement between the results. The standard deviation (STD) of about 0.6 m is in line with indications coming from previous results [Perissin and Rocca, 2006; Crosetto et al., 2010] proving the potential of PSI to provide sub-

metric precision of height measurements. The present figure could even be overestimated due to the non perfect coincidence of the scattering centres measured for the same target by the two acquisition modes (Stripmap and Spotlight) which have different sizes of the resolution cell.

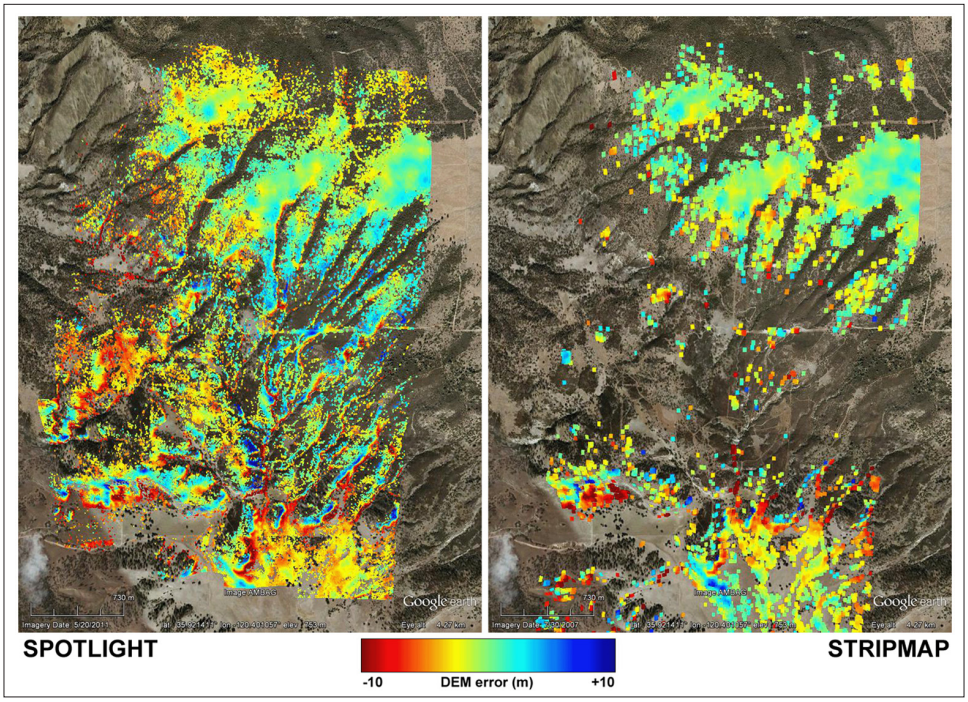


**Figure 3 - Height corrections with respect to an SRTM DEM at 1 arcsec computed by using CSK Spotlight (left) and Stripmap (right) data.**

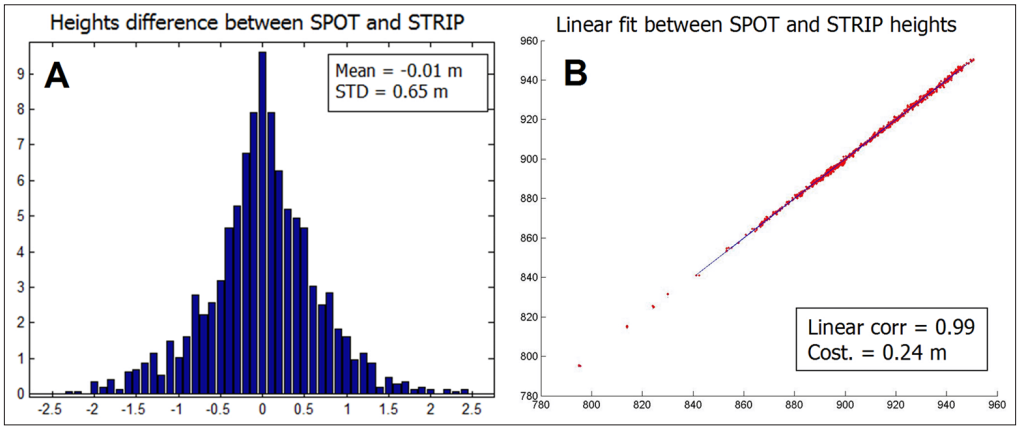


**Figure 4 - (A) Histogram of the differences between heights computed by processing Spotlight and Stripmap data. (B) Scatter plot between the heights measurements derived by the two datasets.**

The correction provided by the multi-temporal analysis is within [-10 m, 10 m] (see color bar in Figure 3). The resolution of the product is that of the input SAR data (1x1 $m^2$ for the Spotlight dataset). The approach is thus able to refine both the accuracy and the spatial resolution of the reference DEM but only where coherent targets are available.

## Exploitation of interferometric tandem-like pairs

In order to assess the potentials of CSK standard interferometry for topographic mapping, 5 CSK Spotlight pairs (listed in Table 1) have been selected according to coherence conditions as well as to the height sensibilities. The latter is defined in terms of height of ambiguity $h_a$ which is inversely proportional to the normal baseline $B_\perp$ [Hanssen, 2001] (all values are reported in Table 1).

**Table 1 - List of tandem-like spotlight pairs selected in the present study.**

| Tandem Pair ID | #1 | #2 | #3 | #4 | #5 |
|---|---|---|---|---|---|
| Master Date | 2010/06/23 | 2010/07/25 | 2010/09/27 | 2010/04/04 | 2010/04/20 |
| Slave Date | 2010/06/24 | 2010/07/26 | 2010/09/28 | 2010/04/05 | 2010/04/21 |
| Master Sensor | CSK-S2 | CSK-S2 | CSK-S2 | CSK-S2 | CSK-S2 |
| Slave Sensor | CSK-S3 | CSK-S3 | CSK-S3 | CSK-S3 | CSK-S3 |
| $B_\perp$ | 38.1 m | 113.5 m | 147.2 m | 317.9 m | 361.2 m |
| $h_a$ | 171.1 m | 57.5 m | 44.3 m | 20.3 m | 18.0 m |

The InSAR processing of high resolution X-band SAR data requires some *ad-hoc* refinements. The more relevant concerns the image alignment which is a crucial step in the interferogram generation process, since 1/8 pixel accuracy is required to avoid significant loss of interferometric phase coherence [Hanssen, 2001]. In case of rough topography and long baselines, standard coregistration methods, based on 2D polynomial modeling of the warp functions, becomes inaccurate, leading to local misregistrations. These effects increase with the spatial resolution of the data [Nitti et al., 2011], thus becoming particularly critical in case of spotlight data. An improved, DEM-assisted image coregistration procedure should be adopted for providing higher-order prediction of the offset vectors [Nitti et al., 2011]. In particular, in the present case, a DEM-assisted approach is strongly recommended due to: i) the high spatial resolution of CSK data; ii) the rough topography; iii) the values of CSK orbital tube diameter which can be longer than 1 km (while TSX rarely exceeds 250m ).
Another source of decorrelation of the interferometric phase [Zebker and Villasenor, 1992] depends on the shift between the Doppler centroid frequencies, $f_{Dc}$, of the tandem-like acquisitions. SAR images acquired by different satellites of the CSK constellation, could show considerable difference between $f_{Dc}$ values. In Figure 5 we report, for each spotlight interferogram of Table 1, the trend along azimuth direction of the difference between the $f_{Dc}$ values of master and slave acquisitions, after coregistration. Difference values are always

above the 30% of the azimuth bandwidth ($B_{az}$~7.9 KHz), due to a systematic shift of about 1.3 km along the track direction, between the ground coverage of images acquired by the satellites S2 (CSK-S2) and S3 (CSK-S3). This misalignment can be explained in terms of different pointing directions of the SAR antennas on the two satellites, and was measured on several others CSK datasets. This source of decorrelation can be minimized by performing a space-variant common-bandwidth filtering of the interferograms.

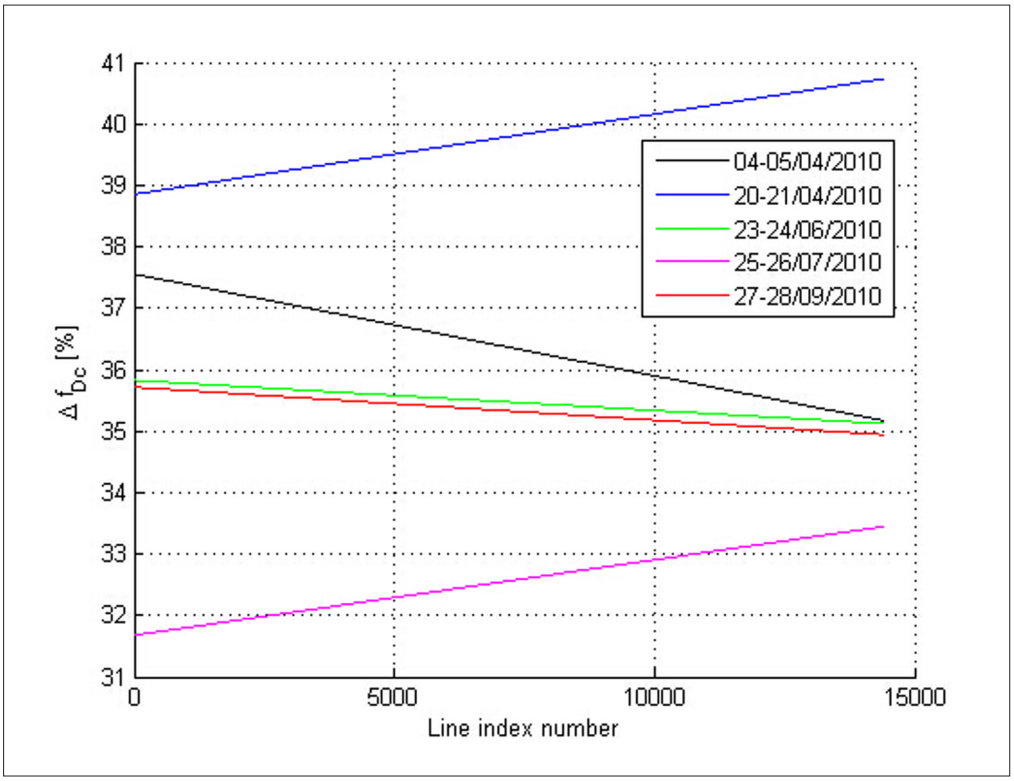


**Figure 5 - Trends of the difference between the $f_{Dc}$ values of master and slave acquisitions, along azimuth direction. The variation of the Doppler centroid frequency along range direction is instead negligible with respect to the azimuth bandwidth.**

The generation of DEM requires the unwrapping of the interferometric phase [Hanssen, 2001]. In order to reduce the interferometric phase gradient and consequently the criticality of phase unwrapping processing, the differential phase field can be used instead of the original one. We generated the differential phase fields by subtracting the reference height derived by the SRTM DEM at 3-arcsec freely available for the area of interest (AOI). The latter was chosen instead of the SRTM DEM at 1-arcsec in order to draw more general conclusions, since the coarser SRTM version is available worldwide within - 60 and 60 degrees of latitude. Figure 6 shows the wrapped DInSAR phase fields of the tandem-like pairs listed in Table 1.

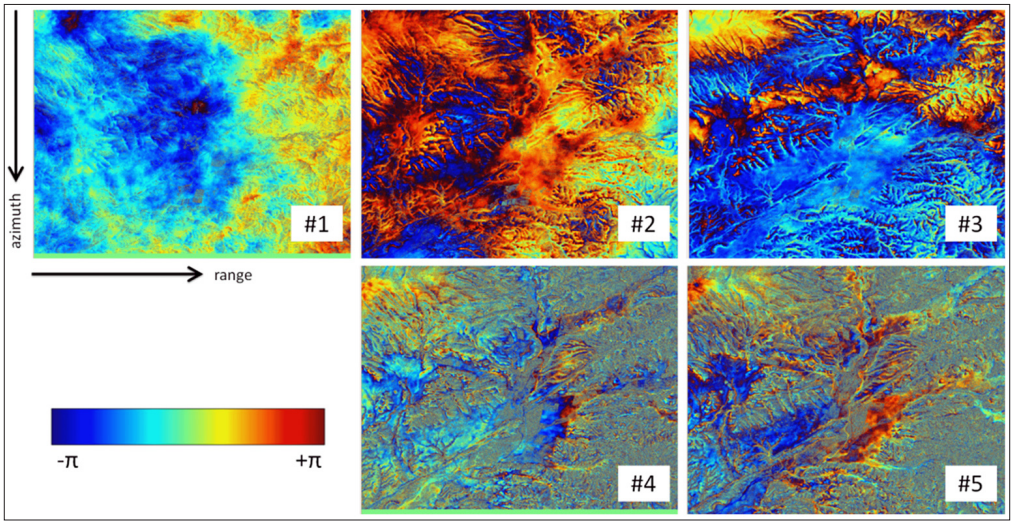


**Figure 6 - Wrapped DInSAR Phase field w/o any filtering.**

A lower interferometric coherence is clearly visible in Figure 6 for the two tandem pairs of April 2010 (in particular for the second one). This coherence loss can be explained in terms of geometrical decorrelation which increases with the spatial baseline and the terrain slope [Hanssen, 2001]. These two pairs indeed have the highest values of $B_{\perp}$ (see Tab. 1), and the low coherence values occur mainly on areas with steep topography. Further contribution to coherence loss is the sensitivity of the short X-band wavelength (3.1 cm) to small changes in the scattering characteristics. METeorological Aerodrome Reports [METAR], released by the two ground meteorological stations closer to the AOI (Paso Robles and Lemoore NAS, respectively 2 and 35 km distant from the stripmap frame), confirm the presence of rain just few hours before the two slave acquisitions of April 2010 (see Tab. 2), which induces changes in the backscattering properties of the soil. Finally, a secondary decorrelation cause can be related to the Doppler centroid separation between master and slave acquisitions which is maximum for these two interferograms as results from Figure 5: in particular for the pair acquired in the second half of April 2010, it reaches the 40% of $B_{az}$.

**Table 2 - 10-hour cumulated rain data (up to acquisition times of April 5 and 21, 2010 SAR images), measured by the two ground meteorological stations closer to the AOI (no precipitation is recorded instead for the other SAR acquisitions of Table 1).**

| Aerodrome | ICAO code | Location | Date: 2010/04/05 | Date: 2010/04/21 |
|---|---|---|---|---|
| Lemoore NAS, CA | KNLC | 36.317°N - 119.950°W | 0.5 mm | 13.5 mm |
| Paso Robles, CA | KPRB | 35.667°N -120.633°W | 2.3 mm | 3.3 mm |

In order to avoid unwrapping artifacts, DInSAR phase fields were pre-filtered through the efficient algorithm proposed by Goldstein and Werner [1998], still preserving a final spatial resolution compatible with HRTI level 3 products (< 12x12 $m^2$). Phase unwrapping was then performed by means of the SNAPHU algorithm [Chen and Zebker, 2001, 2002].

Because of 1 day separation between the tandem-like acquisitions as well as the geophysical setting of the AOI, no ground displacements are expected. Hence, the differential phase is related mainly to the residual topography and to the difference between atmospheric conditions at the times of the two acquisitions. Since our goal is the refinement of the reference DEM by measuring the residual topography, we need to identify and to filter out the atmospheric contributions to the interferometric phase. To this aim we adopted two different strategies: the use of NWP models, discussed in the next section, and the *ad hoc* filtering of the differential phase field. This latter exploits the good coherence level of tandem-like pairs (low temporal decorrelation) and the well known spatial statistical properties of the SAR phase delay induced by the low atmosphere [Hanssen, 2001]. In particular, we estimated the atmospheric signal by filtering the unwrapped DInSAR phase through an adaptive Gaussian low-pass filtering [Wei et al., 2010]. The hypothesis underlying this approach is that the low pass component of the topography is properly removed by the reference DEM subtraction performed during the differential processing [Crosetto et al., 1999]. If so, the main components of the differential phase would be the atmospheric signal and the high pass component of the topographic phase.

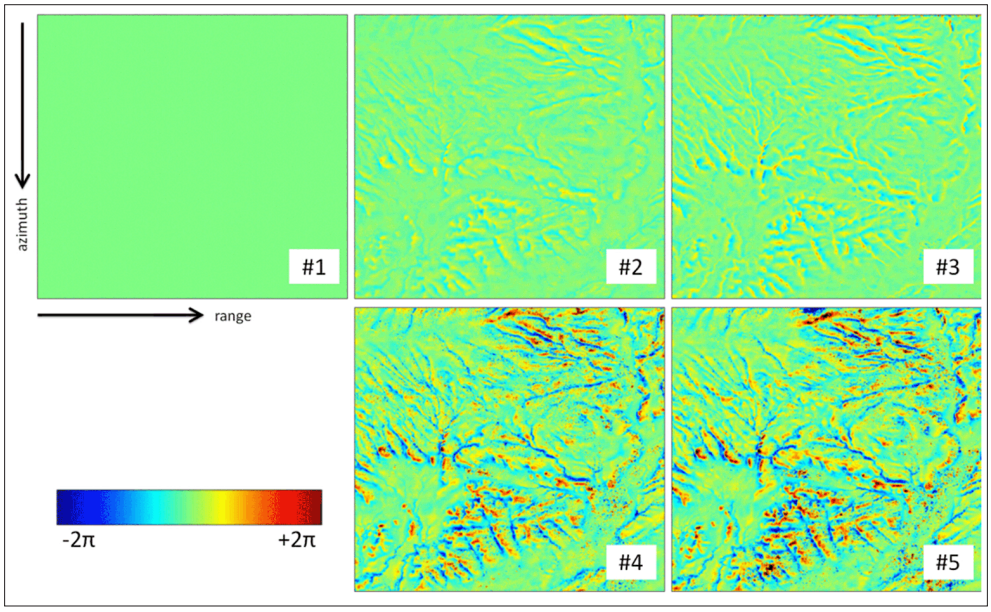


**Figure 7 - Residual topography after APS removal through adaptive low-pass filtering. Orographic features are much more evident for longer baselines, because of the higher height sensitivity.**

Figure 7 shows for all tandem pairs listed in Table 1 the residual topography computed by subtracting from the differential phase the output of the low pass filter and then by applying the phase to height conversion.

The interferometric DEMs were then obtained by combining the smooth SRTM DEM information (used for generating the differential interferograms) with these high-resolution residues provided by the filtered Spotlight interferograms.

***Result analysis***

In order to evaluate the quality of the interferometric DEMs derived in the previous section, we used as benchmark the heights inferred through a PSI multi-temporal analysis which, as detailed previously, result highly reliable. The vertical precision of the interferometric DEM was evaluated in terms of standard deviation (STD) of the height differences computed with respect to the PSI estimations.

Let us discuss first the results achieved through the adaptive filtering approach. The trend of the standard deviations of height differences as function of the corresponding normal baselines $B_{\perp}$ is plotted on the left of Figure 8 for both the unfiltered and filtered products.

The interferometric height precisions are always better than those achieved over the specific AOI by both SRTM products at 3- and 1-arcsec (DTED levels 1 and 2, respectively), as shown in Figure 8. The only exception is represented by tandem-like pair #1, due to its very poor height sensitivity.

Apart from the July 2010 tandem pair (labeled #2 in Table 1), STD values – after filtering – exhibit a decreasing trend with $B_{\perp}$, as expected due to the increasing height sensitivity.

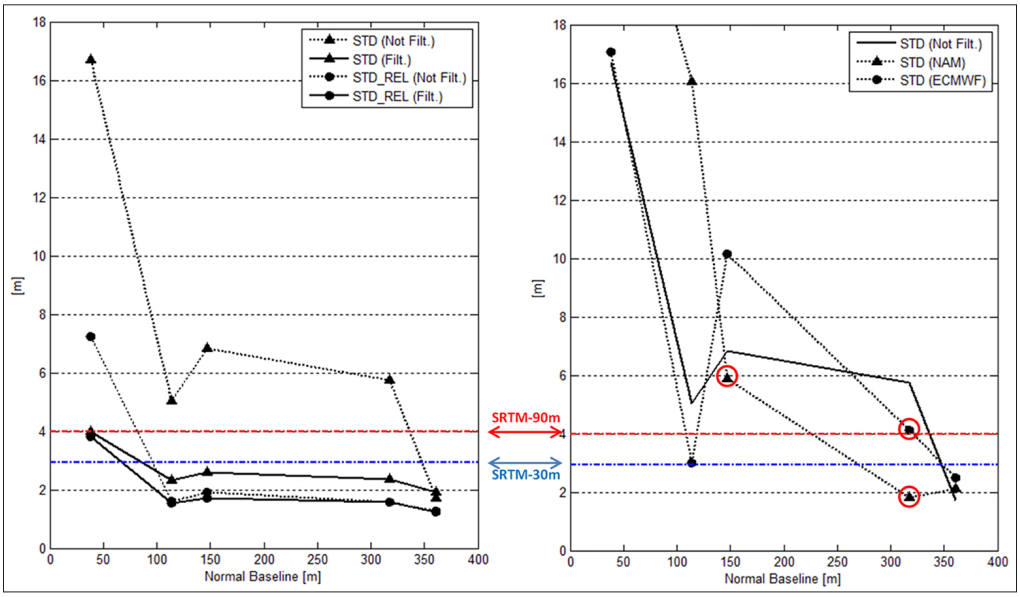


**Figure 8 - (Left) Performances of the adaptive filtering are expressed in terms of STD and STD_REL values of the differences between the heights derived through multi-temporal analysis and tandem-like processing pairs (line). (Right) Performances of the APS mitigation approach through RAMS predictions are expressed in terms of STD values of the height difference with respect to results of the PSI analysis for both NAM and ECMWF boundary conditions.**

Tandem-like pair #2 behaves even better than what we would expect according to its baseline: this is most likely due to the limited Doppler decorrelation affecting this pair with respect to the others (Fig. 5).

By further inspecting Figure 8, we may conclude that the adaptive Gaussian filtering

improves the height precision of all interferometric DEMs. The mitigation of atmospheric artifacts is obviously more evident for shorter baselines, where, due to the low height sensitivity, the atmospheric signal dominates the interferometric phase.
The filtering leads to a considerable improvement also for the tandem-like pair #3 and #4 which show a final STD below 3m. For the interferometric DEM #5, derived from the tandem pair with the longest $B_{\perp}$ (>350 m), the STD value after filtering is even lower than 2 m, but the benefit due to the adaptive filtering is in this case much less appreciable. Possible concurrent causes for this behavior are a particularly smooth spatial distribution of the atmospheric signal, and the long baseline which makes the topographic component of the interferometric phase stronger than the atmospheric signal.
In order to characterize the relative, or point-to-point, vertical accuracy of the interferometric products, we adopted a second figure of merit, referred hereafter as STD_REL, consisting in the standard deviation of the differences of the relative heights between neighboring pixels [Gesch, 2007].
For each PS pixel an unique neighboring pixel coming from the tandem-like interferometric processing was identified resulting in a set of 108000 pairs. No reference control point appears in more than one pair in order to ensure statistical independence of the measures. Distance between neighboring points has been selected to range between 70 m and 100 m. Hence, because of the spatial low-frequency characteristic of the APS signal, turbulences are not expected to significantly affect STD_REL values. Therefore, this figure may be able to check whether or not the adaptive filtering was capable to adequately preserve the high-frequency signal related to the residual topography while filtering out the atmospheric phase artifacts. The values reported in Figure 8 show that STD_REL never worsen after the filtering thus confirming the reliability of the procedure. In particular, the standard deviation of relative differences is around 1.2 m for tandem pair #5, i.e. less than 2 m in terms of 90% confidence level.
These results indicate that normal baselines higher than 300 m are required for fulfilling the HRTI Level 3 specifications on the relative vertical accuracy when generating interferometric DEMs with COSMO/SkyMed in tandem-like configuration. The theoretical study in [Krieger et al., 2005] carried out for the TDX mission, estimates a minimum value for normal baseline of about 150 m (for a monostatic configuration). The higher value measured in our case can be explained in terms of both temporal and Doppler decorrelations which can be neglected in the case of TDX mission.

## Exploitation of interferometric tandem-like pairs

In this section we investigate the potentials of NWP models to provide independent estimates of the Atmospheric Path Delay (APD) suitable to mitigate the interferometric phase artifacts (estimated by the APS) due to the hydrostatic and turbulent components of the lower layers of the atmosphere. This issue has recently become of great interest among experts of SAR interferometry and thus it deserves more investigations.
The NWP models provide 3D fields of all the atmospheric variables influencing the refractive index at the SAR acquisition time. These outcomes are used to compute over the 3D terrain grid the scaled-up refractive index $N = 10^6(n-1)$. According to [Rüeger, 2002a], in the typical SAR bands (L, C and X) the refractivity index can be expressed through

a closed-form formula which accounts for the hydrostatic ($N_{hyd}$), the wet ($N_{wet}$) and the ionosphere ($N_{iono}$) components expressed as follows [Fornaro and Paglia, 2012]:

$$N_{\mathrm{hyd}} = k_1 \frac{P}{T} \quad , \quad N_{\mathrm{wet}} = k_2^n \frac{e}{T} + k_3 \frac{e}{T^2} + k_4 W_{\mathrm{cloud}} \quad , \quad N_{\mathrm{iono}} = k_5 \frac{n_e}{f^2} \quad [1]$$

where $P$ is the total pressure (mbar), $T$ is the temperature (K), $e$ is the water vapor partial pressure (mbar), $f$ is the radar frequency, $n_e$ is the electronic density of the ionosphere and $W_{cloud}$ is the cloud water content (g m$^{-3}$).

Coefficients $k_1$ , $k_2$ , and $k_3$ have been determined empirically in different studies as discussed in [Rüeger, 2002b]. The National Centers of Environmental Prediction (NCEP) has recently adopted for operational use [Cucurull, 2009] the values proposed in [Bevis et al., 1994] because able to provide the better forecast scores. The same values for $k_1$, $k_2$, and $k_3$ coefficients were used in the present study ($k_1$=77.60 K mbar$^{-1}$, $k_2$=70.4 K mbar$^{-1}$, with $k_2'' = k_2 - k_1$, and $k_3$=3.739×10$^5$ K$^2$ mbar$^{-1}$), while $k_4$=1.45 m$^3$g$^{-1}$ was derived from [Solheim et al., 1999].

The integration of the first contribution ($N_{hyd}$) on the vertical profile may reach absolute values generally close to 2-2.5 m; however, its spatial variability is rather limited except for rough topography, where the vertical stratification can be predominant [Hanssen, 2001]. The wet contribution $N_{wet}$ is one order of magnitude lower than the previous one but its spatial and temporal variability is much higher [Fornaro and Paglia, 2012]. Water vapor partial pressure and cloud water content can be computed from the water vapor mixing ratio and the cloud water mixing ratio which are products of NWP models.

Finally, the $N_{iono}$ component can be neglected for CSK enhanced-spotlight acquisitions because of the high X-band carrier frequency ($f$ = 9.6 GHz) and the limited swath extension (only 10x10 km$^2$).

In the present work, numerical weather simulations were performed using the Regional Atmospheric Modeling System (RAMS), a finite-difference, primitive equation, three-dimensional non-hydrostatic mesoscale model, originally developed at Colorado State University [Pielke et al., 1992]. RAMS offers a large selection of parameterizations for turbulent diffusion, solar and terrestrial radiation, moist processes, cumulus convection, etc... making this model particularly suitable for small scale features representation: boundary layer eddies (10-100 m grid spacing), sub-microscale turbulent flow over buildings (1 m grid spacing) and direct wind tunnel experiments (1 cm grid spacing), have been successfully simulated with this code [Tremback and Walko, 2004].

The configured RAMS domain for this study is shown in Figure 9. It includes three nested grid with increasing spatial resolutions (10 km, 2.5 km and 500 m, respectively). Moreover, 17 vertical levels were used in the model within the Atmospheric Boundary Layer depth (ABL) in order to properly model the spatial variability of the water vapor which is mainly concentrated there [Liu et al., 2011].

The selected option for long-wave and short-wave radiation parameterizations was the scheme proposed by Chen and Cotton [1983] that – at expense of a higher computational cost - takes into account the amount of condensate present in the simulated atmosphere.

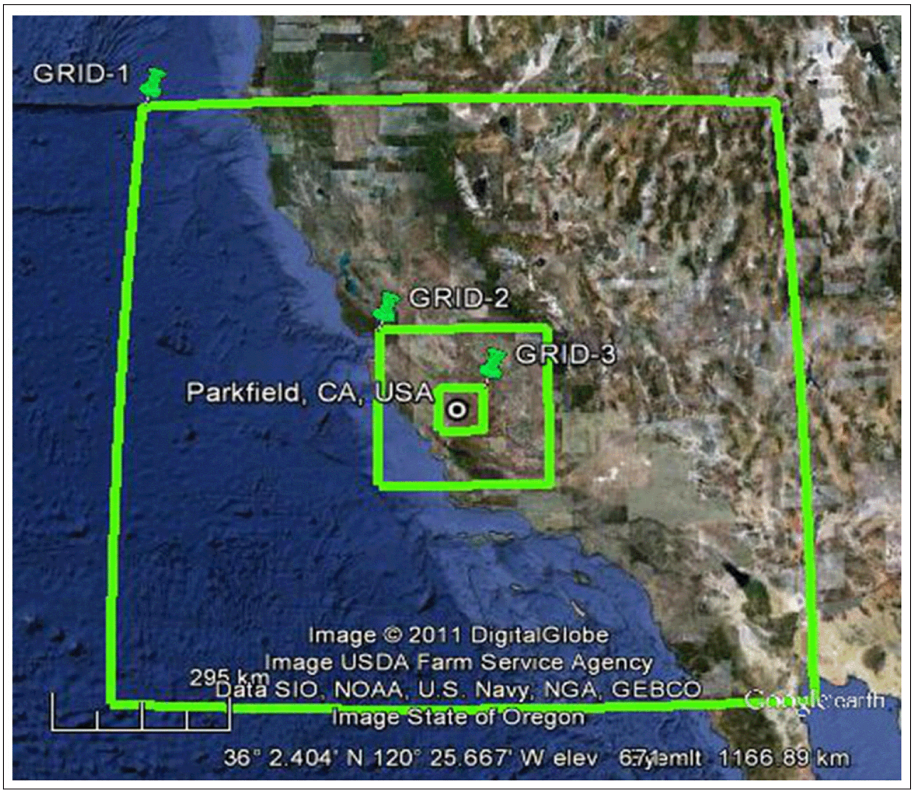


**Figure 9 - RAMS domain. Three nested grid are defined with spatial resolutions of 10 km, 2.5 km and 500 m, respectively.**

In order to investigate the potentials of NWP modeling as operational instrument for the mitigation of atmospheric artifacts in SAR interferometry, and due the lack of sounding stations close to the area covered by the CSK images, RAMS was cold-started in all our simulations. NWP models that are cold-started without a data assimilation scheme require a "spin-up" time period even longer than 24h for small-scale features (such as water vapor spatial variation) to develop [Liu et al., 2011]. According to this, RAMS was set to cover a time-span of ~ 50h, starting at 00:00 UTC of the day before the CSK-S2 acquisition (occurring at 02.10 UTC) and ending at the tandem CSK-S3 acquisition time.

Besides the model parameters, the boundary condition could play a crucial role as well. To assess the impact of initial and boundary conditions on the delay predictions, both analysis fields provided by the European Centre for Medium-Range Weather Forecasts (ECMWF) and North American Mesoscale model (NAM) have been used for simulations, without changing the model settings. NAM data are provided by NCEP with a spatial resolution (12 km) and a number of pressure levels (39, between 50 and 1000 mbar) twice better than ECMWF.

The APD prediction for each SAR acquisition was computed by integration of the refractive index profile $N(r)$ along the Line of Sight (LOS):

$$APD = 10^{-6} \int_{LOS} N(r)\,dr \quad [2]$$

Since elevation angles are always well above 15 deg for all satellite SAR sensors, the bending of the wave path may be neglected [Hanssen, 2001].The actual integration path direction is computed pixel by pixel according to the ground profile and to the satellite orbital position. The interpolation of the 3D refractive index field along the LOS is performed through an inverse distance algorithm, with an increasing spacing from the target on ground towards the satellite, following the staggered vertical coordinate system adopted by RAMS.
Figure 10 shows an example of APD field predicted by RAMS for the acquisition time of the April 21, 2010 image, as well as the scatter plots of the single hydrostatic and wet components with respect to topographic profile (relative to a reference point). As expected, the hydrostatic contribution is highly correlated with topography, while correlation is weak for the wet component.
By further comparing RAMS outcomes obtained with NAM and ECMWF boundary conditions, we report in Figure 11 the spatial mean of the differences between the APD values computed by using the two different boundary conditions. The APD was computed along the zenith direction and separately for the hydrostatic and wet components of the atmosphere. The error bars are proportional to the STD of the differences. The differences for the hydrostatic component are in the order of few millimeters, while they become much higher (even in the order of several centimeters) in the case of wet delay. This demonstrates that delay predictions may vary considerably given different boundary conditions.

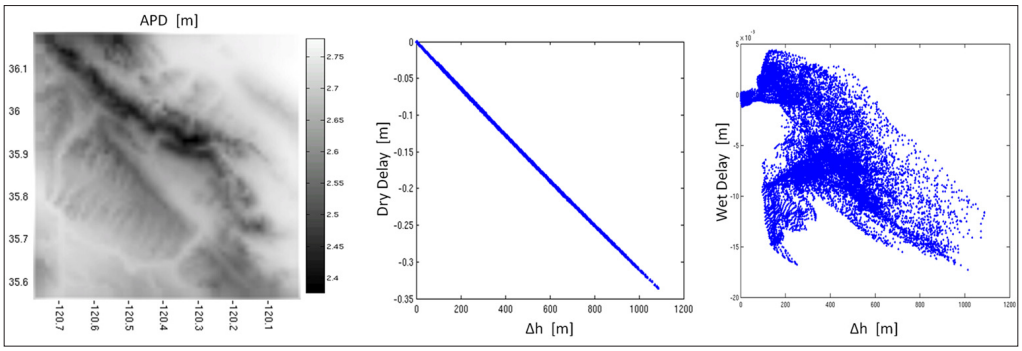


**Figure 10 - (Left) APD derived from RAMS predictions for April 21, 2010 at ~ 02:10 UTC (boundary conditions provided by NAM analysis field). (Center) Scatter plot of the hydrostatic contribution with respect to topography. (Right) Scatter plot of the wet contribution.**

These results, deeply discussed later on, are in line with other recent works [Liu et al., 2011], and point out the major limit in using NWP models for atmospheric component mitigation in SAR interferometry which is related to the centimetric accuracy of the wet delay prediction. This is one order of magnitude higher than that required to properly filter the interferoemtric phase. In fact, by requiring a sub-meter height accuracy:

$$h^{e}_{Atm} \leq 1m \quad [3]$$

and considering the most favorable case of tandem pair #5, which has the highest height sensitivity ($h_a$=18 $m$), the constraint on the error in slant delay is:

$$\Delta\rho^{e}_{Atm} = \frac{\lambda}{2}\frac{h^{e}_{Atm}}{h_a} \leq 0.833mm \quad [4]$$

Then, assuming independent errors for master and slave, the requirement for the zenith delay accuracy is:

$$\delta^{e}_{APD} = 0.5 \times \Delta\rho^{e}_{ADP} \times \cos\theta_{inc} \leq 0.349mm \quad [5]$$

In order to evaluate the performances of RAMS in predicting the troposphere behavior, we used the radiosonde records (RAOBS) which are one of the standard observations of water vapor [Liu et al., 2011]. Since radiosonde stations are totally absent over the CSK frames, the comparison has been carried out over the *San Diego* area, where it is installed the closest radiosonde to the AOI (Station ID: 72293 NKX; lat: 32.85°N, lon: 117.11°W). We used 4 RAOBS records from this site to evaluate the corresponding RAMS predictions, relative to different dates and times.

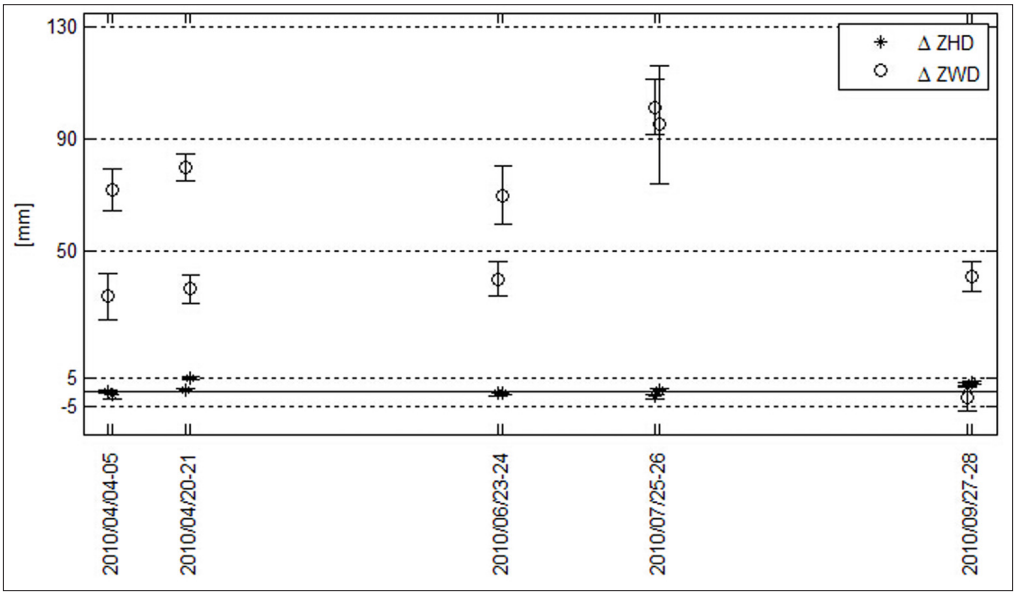


**Figure 11 - Comparison of zenith signal delay components computed from RAMS predictions with NAM and-ECMWF boundary conditions. A very good agreement is found for the hydrostatic contribution (differences less than 5 mm), while ZWD differences may exceed 10 cm.**

The direct comparison between NWP model outputs and observations presents numerous difficulties [Buckley et al., 2004]. The major one is related to the fact that the NWP model outcomes are spatially averaged over a grid volume while the observations represent point measurements. That's why we preferred to use for the boundary conditions the NAM data which have higher resolution than ECMWF. RAMS configuration has not been modified during the validation tests with respect to the simulations previously discussed.
The statistics of the results (see Figure 12) indicate that RAMS slightly underestimates the total pressure, the air temperature and the water vapor mixing ratio in mean by 9.3 mbar, 0.6 K and 0.25 g/kg, respectively. The corresponding standard deviations are 9.4 mbar, 1.62 K and 0.89 g/kg, respectively. According to [1], the deviations of the RAMS outcomes with respect to observations tend to cancel out when used for computing, in particular, the hydrostatic component of the refractive index.

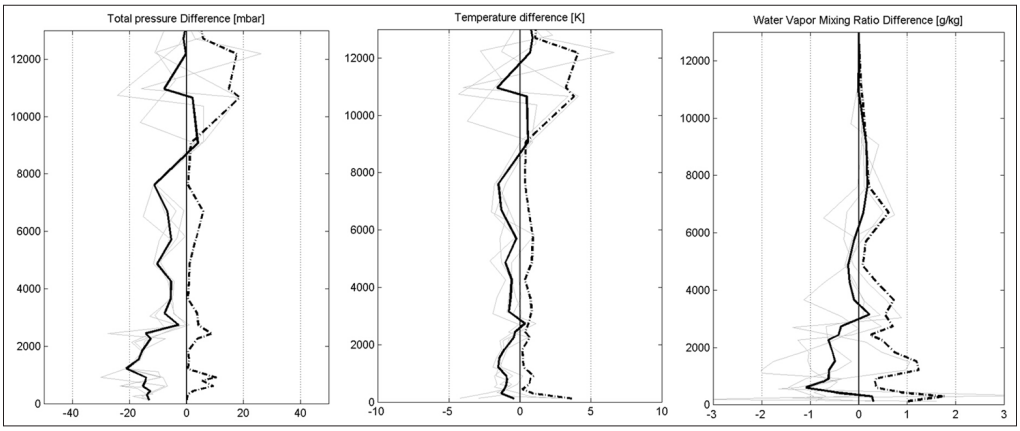


**Figure 12 - Comparison between RAMS predictions and RAOBS records (radiosonde 72293 NKX, San Diego). Vertical profiles of (left) total pressure [mbar], (centre) air temperature [K] and (right) water vapor mixing ratio [g/kg] difference between RAMS and RAOBS: solid and dashed bold lines represent mean profile and standard deviation trend along the profile, respectively. Vertical axes represent altitudes in meters.**

Results from the above analysis are comparable with the outcomes of different NWP models, like WRF, as reported by recent studies [Liu et al., 2011]. We may conclude that RAMS is capable to provide reliable predictions of the state variables influencing the value of the refractive index. Nevertheless, we need still to assess whether the accuracy of the slant delay pattern derived from RAMS predictions is millimetric (as required for an operational use of NWP models for the mitigation of the phase artifacts in X-band SAR interferometry) or worse.
To this aim the APD derived from RAMS has been integrated along zenith direction and compared with independent GPS Zenith Total Delay (ZTD) data obtained for sixty GPS stations of the UNAVCO consortium available within the inner grid in Figure 9. GPS ZTD measurements range between 2.0 and 2.3 m. The experiment has been repeated for different times dates and seasons of the year 2010 (see Nitti et al., [2012] for details). Negligible biases have been found between GPS ZTD data and ZTD measurements predicted with

RAMS, with a centimetric RMSE (independent from the boundary conditions). Since ZTD data provided by GPS have millimetric accuracy [Zumberge et al., 1997], we may conclude that the accuracy achievable with NWP models is one order of magnitude worse, in line with the conclusions of recent scientific works [Gong et al., 2011]. APS mitigation through NWP models seems therefore to be still unfeasible especially for X-band SAR interferometry, where a millimetric accuracy is required because of the short radar wavelength (λ~3 cm).
This conclusion is confirmed by looking at the STD of the height difference between the height values derived from PSI and those obtained by using NWP model predictions to remove APS (see right panel in Figure 8). RAMS performances tend to vary considerably from one interferogram to another and by changing the boundary conditions. In few specific cases (circled in red on the right of Figure 8), quite mitigation of the atmospheric artifacts is noticeable, but in all the other tests the height accuracy is strongly worsened. Moreover, the adaptive filtering provides always better performances than using RAMS. As confirmed by recent works in C-band [Liu et al., 2011], the role of weather models for delay mitigation may change oppositely from a delay mitigating to an error contributor.
Previous results lead anyway to the conclusion that NWP simulations performed with boundary conditions provided by global models, even if not suitable for atmospheric artifacts mitigation, may however represent an operational instrument for improving the absolute horizontal accuracy of spotlight PS maps. No information is indeed provided in the annotations of CSK products for the atmospheric path delay, while TSX offers at least constant additional corrections [Schubert et al., 2010] that may not guarantee sub-pixel accuracy in case of rough topography.

## Conclusions

This work is aimed at experimenting the potentials of CSK in measuring ground elevation as well as to assess the feasibility of using numerical weather models to mitigate the atmospheric artefacts affecting the interferometric phase. The latter in recent years has become an issue of increasing interest thus deserving more investigations and a final assessment.
We first processed through SPINUA PSI algorithm a stack of CSK data acquired over Parkfield (California, USA), measuring with meter accuracy the ground elevation of available coherent targets. Then we used this measurements as reference values to check the accuracy of the height values obtained by processing 5 tandem-like CSK Spotlight pairs with different height sensitivities. In order to suppress the atmospheric artefacts affecting the interferometric phase we experimented both a classical spatial filtering of the differential phase field as well as the use of the atmospheric fields derived by running the NWP model RAMS.
The outcomes indicate that by properly filtering the differential interferometric phase derived by using CSK tandem-like pairs with normal baselines higher than 300 m, it is possible to derive DEMs fulfilling the HRTI Level 3 specifications on the relative vertical accuracy. These results would be even improved by reducing the Doppler decorrelation affecting the CSK tandem-like pairs due a systematic shift of 1.3 km along the azimuth direction. Moreover, the temporal decorrelation, due to the one day separation between acquisitions, can be mitigated by selecting images acquired during dry seasons which strongly limit the changes in soil properties.
Concerning the mitigation of atmospheric artifacts through NWP models, the RAMS model was used to generate and remove from the DInSAR phase the atmospheric contribution to

the SAR signal. The RAMS outcomes were compared with independent measurements from GPS and radiosondes, and the final height values validated by using the reference PSI measurements as done for the filtering approach. Results indicate that the use of NWP models it is still unfeasible especially for X-band SAR interferometry. SAR processing indeed requires millimetric accuracy in the zenith atmospheric delay while the outcomes of the numerical models are in the order of centimenters even using RAMS model which is suitable also for small scale features representation. Possible improvements can derive by the assimilation of surface observations and soundings in the RAMS weather modeling.

## Acknowledgements

Work supported by ASI (Agenzia Spaziale Italiana) in the framework of the project "AO-COSMO Project ID-1462 - Feasibility of possible use of COSMO/SkyMed in bistatic SAR Earth observation - ASI Contract I/063/09/0".

## References

Bamler R., Eineder M., Adam N., Gernhardt S., Zhu X. (2009) - *Interferometric Potential of High Resolution Spaceborne SAR*. Photogrammetrie - Fernerkundung - Geoinformation (PGF), 5/2009: 407-419.

Battazza F., Ciappa A., Coletta A., Covello F., Manoni G., Pietranera L., Valentini G. (2009) - *COSMO/SkyMed Mission: a set of X-band SAR Applications conducted during 2008*. Rivista Italiana di Telerilevamento, 41 (3): 7-21.

Berardino P., Fornaro G., Lanari R., Sansosti E., (2002) - *A new algorithm for surface deformation monitoring based on small baseline differential SAR interferograms*. IEEE Transactions on Geoscience and Remote Sensing, 40 (11): 2375-2383. doi: http://dx.doi.org/10.1109/TGRS.2002.803792.

Bevis M., Businger S., Chiswell S., Herring, T.A., Anthes R.A., Rocken C., Ware R.H. (1994) - *GPS Meteorology: Mapping Zenith Wet Delays onto Precipitable Water.* Journal of Applied Meteorology, 33 (3): 379-386. doi: http://dx.doi.org/10.1175/1520-0450(1994)033<0379:GMMZWD>2.0.CO;2.

Bovenga F., Refice A., Nutricato R., Guerriero L., Chiaradia M.T. (2004) - *SPINUA: a flexible processing chain for ERS/ENVISAT long term interferometry.* Proceedings of Envisat & ERS Symposium, Salzburg, Austria, 6-10 September 2004. ESA SP-572, CD-ROM, ISBN: 92-9092-883-2.

Bovenga F., Nutricato R., Refice A., Wasowski J. (2006) - *Application of Multi-temporal Differential Interferometry to Slope Instability Detection in Urban/Peri-urban Areas.* Engineering Geology, 88 (3-4): 218-239. doi: http://dx.doi.org/10.1016/j.enggeo.2006.09.015.

Bovenga F., Wasowski J., Nitti D.O., Nutricato R., Chiaradia M.T. (2012) - *Using Cosmo/SkyMed X-band and ENVISAT C-band SAR Interferometry for landslide analysis.* Remote Sensing of Environment, 119: 272-285. doi: http://dx.doi.org/10.1016/j.rse.2011.12.013.

Buckley R.L., Weber A.H., Weber J.H. (2004) - *Statistical comparison of Regional Atmospheric Modelling System forecasts with observations.* Meteorological Applications, 11: 67-82. doi: http://dx.doi.org/10.1017/S1350482703001142.

Chen C., Cotton W.R. (1983) - *A one-dimensional simulation of the stratocumulus-capped mixed layer.* Boundary-Layer Meteorology, 25: 289-321. doi: http://dx.doi.org/10.1007/BF00119541.

Chen C.W., Zebker H.A. (2001) - *Two-dimensional phase unwrapping with use of statistical models for cost functions in nonlinear optimization*. Journal of the Optical Society of America, 18: 338-351. doi: http://dx.doi.org/10.1364/JOSAA.18.000338.

Chen C.W., Zebker H.A. (2002) - *Phase unwrapping for large SAR interferograms: Statistical segmentations and generalized network models*. IEEE Transactions on Geoscience and Remote Sensing, 40: 1709-1719. doi: http://dx.doi.org/10.1109/TGRS.2002.802453.

Covello F., Battazza F., Coletta A., Battagliere M.L., Bellifemine V., Candela L. (2010) - *One-day interferometry results with the COSMO/SkyMed constellation*. Proceedings of IGARSS 2010, 25-30 July, 2010, Honolulu, Hawaii, (USA).

Crosetto M., Pérez Aragues F. (1999) - *Radargrammetry and SAR interferometry for DEM generation: validation and data fusion*. Proceedings of CEOS SAR Workshop, ESA-CNES, Toulouse, France, 1999.

Crosetto M., Monserrat O., Iglesias R., Crippa B. (2010) - *Persistent Scatterer Interferometry: Potential, Limits and Initial C and X-band Comparison.* Photogrammetric Engineering and Remote Sensing, 76 (9): 1061-1069.

Cucurull L. (2009) - *Improvement in the Use of an Operational Constellation of GPS Radio Occultation Receivers in Weather Forecasting*. Weather and Forecasting, 25: 749-767. doi: http://dx.doi.org/10.1175/2009WAF2222302.1.

Ferretti A., Prati C., Rocca F. (2001) - *Permanent scatterers in SAR Interferometry.* IEEE Transactions on Geoscience and Remote Sensing, 39: 8-20. doi: http://dx.doi.org/10.1109/36.898661.

Fornaro G., Paglia L. (2012) - *A comparison of atmospheric phase delay estimated by ASAR and MERIS over the Campania area.* International Journal of Remote Sensing, 33 (5): 1507-1528. doi: http://dx.doi.org/10.1080/01431161.2011.578598.

Gesch D.B. (2007) *Chapter 4 – The National Elevation Dataset*, in Maune D., *Digital Elevation Model Technologies and Applications: The DEM Users Manual*, 2nd Edition: Bethesda, Maryland, ASPRS: 99-118.

Goldstein R.M., Werner C.L. (1998) - *Radar interferogram filtering for geophysical applications.* Geophysical Research Letters, 25 (21): 4035-4038. doi: http://dx.doi.org/10.1029/1998GL900033.

Gong W., Meyer F., Liu S. (2011) - *Numerical Weather Model Assisted Time Series InSAR Processing for Geophysical Application*. Proceedings of Fringe 2011. ESA/ESRIN, Frascati, Italy.

Hanssen R. (2001) - *Radar Interferometry: Data Interpretation and Error Analysis.* Kluwer Academic Publishers, Dordrecht, The Netherlands. pp. 308.

Krieger G., Fiedler H., Hajnsek I., Eineder M., Werner M., Moreira A. (2005) - *TanDEM-X: Mission Concept and Performance Analysis*. IEEE Proceedings of IGARSS 2005, 7 (4890-4893). doi: http://dx.doi.org/10.1109/IGARSS.2005.1526770

Krieger G., Moreira A., Fiedler H., Hajnsek I., Werner M., Younis M., Zink M. (2007) - *TanDEM-X: A Satellite Formation for High-Resolution SAR Interferometry*. IEEE Transaction of Geoscience and Remote Sensing, 45 (11): 3317-3341, November 2007. doi: http://dx.doi.org/10.1109/TGRS.2007.900693.

Liu S., Mika A., Gong W., Hanssen R., Meyer F., Morton D., Webley P.W. (2011) - *The role of weather models in mitigation of tropospheric delay for SAR interferometry.* Proceedings of the 2011 IEEE International Geoscience and Remote Sensing Symposium, Vancouver, BC. pp: 2562 - 2565. doi: http://dx.doi.org/10.1109/IGARSS.2011.6049735.

National Imagery and Mapping Agency (NIMA) (2000) - *High Resolution Terrain Information (HRTI): Performance Specification*. MIL-PRF-89048.

Nitti D.O., Hanssen R.F., Refice A., Bovenga F., Nutricato R. (2011) - *Impact of DEM-Assisted Coregistration on High-Resolution SAR Interferometry.* IEEE Trans. on Geoscience and Remote Sensing, 49: 1127-1143. doi: http://dx.doi.org/10.1109/TGRS.2010.2074204.

Nitti D. O., Nutricato R., Intini F., Bovenga F., Chiaradia M. T., Pacione R., Vespe F. (2012) - *On the use of weather models in the mitigation of atmospheric artifacts in X-band SAR Interferometry*. EGU General Assembly 2012. Vienna, Austria.

Perissin D., Rocca F. (2006) - *High-Accuracy Urban DEM Using Permanent Scatterers*. IEEE Transactions on Geoscience and Remote Sensing, 44 (11): 3338-3347. doi: http://dx.doi.org/10.1109/TGRS.2006.877754.

Pielke R. A., Cotton W. R., Walko R. L., Tremback C. J., Lyons W. A., Grasso L. D., Nicholls M. E., Moran M. D., Wesley D. A., Lee T. J., Copeland J. H. (1992) - *A comprehensive meteorological modeling system - RAMS*. Meteorology and Atmospheric Physics, 49: 69-91. doi: http://dx.doi.org/10.1007/BF01025401.

Prati C., Ferretti A., Perissin D. (2010) - *Recent advances on surface ground deformation measurement by means of repeated space-borne SAR observations*. Journal of Geodynamics, 49: 161-170. doi: http://dx.doi.org/10.1016/j.jog.2009.10.011.

Rabus B., Eineder M., Roth A., Bamler R. (2003) - *The Shuttle Radar Topography Mission, A new class of digital elevation models acquired by spaceborne radar*. ISPRS Journal of Photogrammetry and Remote Sensing, 57 (4): 241-262. doi: http://dx.doi.org/10.1016/S0924-2716(02)00124-7.

Reale D., Nitti D.O., Peduto D., Nutricato R., Bovenga F., Fornaro G. (2011) - *Post-seismic deformation monitoring with the COSMO/SkyMed constellation*. Geoscience and Remote Sensing Letters, 8 (4): 696-700. doi: http://dx.doi.org/10.1109/LGRS.2010.2100364H.

Rüeger J.M. (2002a) - *Refractive Index Formulae for Electronic Distance Measurement with Radio and Millimetre Waves*. Unisurv Report S-68, School of Surveying and Spatial Information Systems, University of New South Wales, UNSW SYDNEY NSW 2052, Australia, pp. 1-52.

Rüeger J.M. (2002b) - *Refractive index formulae for radio waves*. Proceedings of the FIG XXII International Congress, Washington, D.C. USA.

Sandwell D.T., Sichoix L. (2000) - *Topographic phase recovery from stacked ERS interferometry and a low-resolution digital elevation model*, Journal of Geophysical Research, 105 (B12): 28,211-28,222. doi: http://dx.doi.org/10.1029/2000JB900340.

Schubert A., Jehle M., Small D., Meier E. (2010) - *Influence of Atmospheric Path Delay on the Absolute Geolocation Accuracy of TerraSAR-X High-Resolution Products*. IEEE Transactions on Geoscience and Remote Sensing, 48 (2): 751-758. doi: http://dx.doi.org/10.1109/TGRS.2009.2036252.

Solheim F. S., Vivekanandan J., Ware R.H., Rocken C. (1999) - *Propagation delays induced in GPS signals by dry air, water vapor, hydrometeors, and other particulates*. Journal of Geophysical Research, 104: 9663-9670. doi: http://dx.doi.org/10.1029/1999JD900095.

Tremback C.J., Walko R.L. (2004) - *Implementing Very-High Resolution Capabilities into a Mesoscale Atmospheric Model: New Capabilities for the Regional Atmospheric Modeling System (RAMS)*. Mesoscale and CFD Modeling for Military Applications, University of Minnesota.

Wei M., Sandwell D., Smith-Konter B. (2010) - *Optimal combination of InSAR and GPS for measuring interseismic crustal deformation.* Advances in Space Research, 46 (2): 236-249. doi: http://dx.doi.org/10.1016/j.asr.2010.03.013.

Zebker H.A., Villasenor J. (1992) - *Decorrelation in interferometric radar echoes.* IEEE Transactions on Geoscience and Remote Sensing, 30 (5): 950-959. doi: http://dx.doi.org/10.1109/36.175330.

Zumberge J.F., Heflin M.B., Jefferson D.C., Watkins M.M., Webb F.H. (1997) - *Precise point positioning for the efficient and robust analysis of GPS data from large networks*, Journal of Geophysical Research, 102 (B3): 5005-5017. doi: http://dx.doi.org/10.1029/96JB03860.

**Received 07/02/2012, accepted 19/12/2012**